

Spatial interference between pairs of optical paths with a chaotic source

Michele Cassano

Dipartimento Interateneo di Fisica, Università degli Studi di Bari, 70100 Bari, Italy

Milena D'Angelo

Dipartimento Interateneo di Fisica, Università degli Studi di Bari, 70100 Bari, Italy
Istituto Nazionale Di Fisica Nucleare, sez. di Bari, 70100 Bari, Italy

Augusto Garuccio

Dipartimento Interateneo di Fisica, Università degli Studi di Bari, 70100 Bari, Italy
Istituto Nazionale Di Fisica Nucleare, sez. di Bari, 70100 Bari, Italy

Tao Peng

Department of Physics, University of Maryland, Baltimore County, Baltimore, MD
21250, USA

Yanhua Shih

Department of Physics, University of Maryland, Baltimore County, Baltimore, MD
21250, USA

Vincenzo Tamma

Institut für Quantenphysik and Center for Integrated Quantum Science and
Technology (IQST), Universität Ulm, D-89069 Ulm, Germany

E-mail: vincenzo.tamma@uni-ulm.de

Abstract. We demonstrate a second-order spatial interference effect with a chaotic source. This phenomenon arises from the spatial indistinguishability between pairs of optical paths emerging from correlation measurements in the photon-number fluctuations, providing a deeper understanding of the physics of multi-photon interference and spatial coherence. We show how this effect can be used to simulate a controlled-*NOT* gate, as well as arbitrary-order on-demand entanglement correlations in more general interferometric networks.

PACS numbers: 42.50.-p,42.50.Ar

1. Introduction

The fundamental physics of temporal and spatial coherence and interference with thermal light is at the very heart of the experiments performed in the mid-1950s by Hanbury Brown and Twiss. These experiments triggered the development of the quantum optics field [1, 2, 3, 4]. Indeed, in the last 60 years, numerous fundamental studies [5, 6, 7, 8, 9, 10] of the physics of multi-photon interference have been performed, with applications in imaging [11, 12, 13, 14, 15, 16, 17], quantum information processing [18, 19, 20, 21, 22], metrology [23, 24], N-photon tomography, entanglement generation [9, 25] and entanglement simulation [26, 27, 28, 29, 30].

Recently, a second-order correlation phenomenon based on the interference between pairs of optical paths has been demonstrated [10] in the temporal domain with a chaotic source, providing a deeper fundamental understanding of the physics of second-order coherence beyond the Hanbury Brown and Twiss effect. As shown in [10], this phenomena can be also used to simulate a controlled-NOT (CNOT) gate operation [31, 32, 33].

In this paper, we demonstrate theoretically a second-order interference effect in the spatial domain analogous to the one demonstrated in the temporal domain [10]. The proposed interferometer (Fig. 1) is characterized by two identical two-pinhole masks illuminated by chaotic light, and placed in two separate arms. The distance between the two pinholes in both masks is larger than the transverse coherence length of the chaotic source. Hence, no first-order interference exists behind each mask. Nonetheless, we show that second-order interference between two pairs of spatially indistinguishable optical paths can be observed by performing correlation measurements at the interferometer output (sect. 2). Furthermore we demonstrate that the proposed interference phenomenon can be used (Fig. 2) to simulate a particular class of controlled-unitary gates, including a CNOT gate. We also propose (sect. 3) a modified setup (Fig. 3) that can be used for the implementation of higher-order interferometric networks.

2. Basic interference effect

In the proposed interferometer (Fig. 1), chaotic light is split by a balanced non-polarizing beam splitter. Two identical two-pinhole masks are placed, in the output arms of the beam splitter, at the same distance z from the source. The pinholes at the positions are indicated as 1,2 for the upper mask and 1',2' for the lower mask. The light transmitted by the masks reaches two point-like detectors, D_C and D_T , placed at the same distance f from the masks. A correlation measurement in the fluctuation of the number of photons is finally performed.

Let us start with the general expression of the second-order correlation function [34, 17]

$$G^{(2)}(x_i, x_j) \propto \langle n(x_i)n(x_j) \rangle = \langle n(x_i) \rangle \langle n(x_j) \rangle + \langle \Delta n(x_i)\Delta n(x_j) \rangle, \quad (1)$$

with $i = 1,2$ and $j = 1',2'$, where n represents the photon number and Δn the

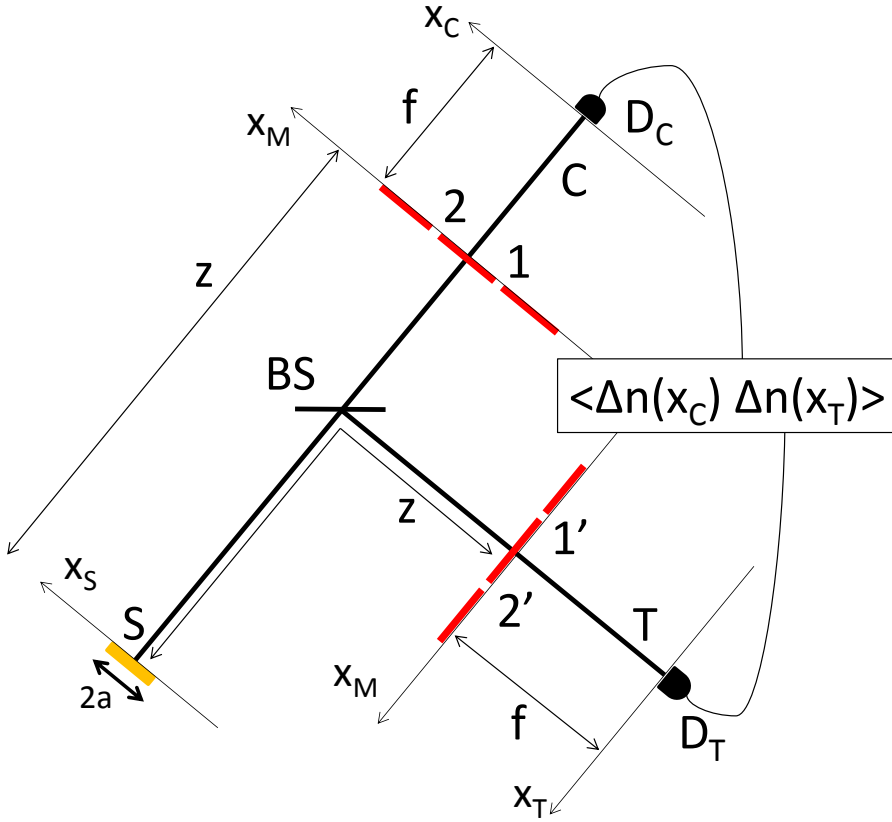


Figure 1. Scheme of the proposed interferometer for observing spatial second-order interference between indistinguishable pairs of optical paths. The light, emitted from a one-dim chaotic sources of size $2a$, after being split on a balanced non-polarizing beam splitter propagates through two identical two-pinhole masks placed at the same distance z from the source and reaches two point-like detectors, D_C and D_T , placed at distance f from the masks. A correlation measurement between the fluctuations of the number of photons detected by D_C and D_T is performed.

photon-number fluctuation around the mean. We consider now the case of a quasi-monochromatic chaotic source, which, for simplicity, is also assumed to be 1-dim, of length $2a$, and H-polarized. The input chaotic light state is described by [34, 35]

$$\hat{\rho}_H = \int \left[\prod_{\kappa} d^2 \alpha_{\kappa, H} \right] P(\{\alpha_{\kappa, H}\}) \bigotimes_{\kappa} |\alpha_{\kappa, H}\rangle_S \langle \alpha_{\kappa, H}|,$$

with the Glauber-Sudarshan probability distribution [3, 36]

$$P(\{\alpha_{\kappa, H}\}) = \prod_{\kappa} \frac{1}{\pi \langle n_{\kappa} \rangle} \exp \left(-\frac{|\alpha_{\kappa, H}|^2}{\langle n_{\kappa} \rangle} \right),$$

where $\alpha_{\kappa, H}$ are H-polarized coherent states, in the mode κ associated with the x component of the transverse wave vector, and $\langle n_{\kappa} \rangle$ is the corresponding average photon number, which is assumed for simplicity to be constant [35]. In this case Eq. (1) reduces

to [13]

$$G^{(2)}(x_i, x_j) = G^{(1)}(x_i)G^{(1)}(x_j) + |G^{(1)}(x_i, x_j)|^2,$$

with $G^{(1)}$ the first-order correlation function. Therefore $G^{(2)}(x_i, x_j)$ depends on two contributions: the first one, $G^{(1)}(x_i)G^{(1)}(x_j)$, is a constant background; the second one, $|G^{(1)}(x_i, x_j)|^2$, is the interference term. The background can be removed by performing a correlation measurement between the fluctuations of the number of photons [17]. Due to the position (or momentum) correlation at the heart of the ghost imaging [13, 14, 15, 16] (or the HBT [1, 2]) effect, the outcome of this measurement [17, 34]

$$\langle \Delta n(x_i) \Delta n(x_j) \rangle \propto |G^{(1)}(x_i, x_j)|^2$$

is different from zero for all the possible pairs of paths $(i, j) = (1, 1'), (2, 2'), (1, 2'), (2, 1')$, provided the relative distance between each pair of pinholes is smaller than the transverse coherence length of the source (l_{coh}), which is: $|x_i - x_j| \ll l_{coh}$. Now an interesting result comes out by working in the hypothesis that

(A) the pinholes, in each mask, are separated by a distance greater than the transverse coherence length of the source, namely

$$|x_1 - x_{2'}| \gg l_{coh} \quad |x_{1'} - x_2| \gg l_{coh}; \quad (2)$$

(B) the corresponding pairs of pinholes at the two masks are within the transverse coherence length, which is

$$|x_1 - x_{1'}| \ll l_{coh} \quad |x_2 - x_{2'}| \ll l_{coh}. \quad (3)$$

In fact, in this case, only the two pairs of paths $(1, 1')$ and $(2, 2')$ (each one associated with two paths spatially coherent with respect to each other), contribute to the correlation, while no contribution comes from the two pairs of paths $(1, 2')$ and $(2, 1')$, namely

$$\langle \Delta n(x_i) \Delta n(x_j) \rangle \neq 0 \Leftrightarrow (i, j) = (1, 1'), (2, 2').$$

What happens if we perform correlation measurements after the two-pinhole masks? Intuitively one may expect that the only two possible contributions, associated with the two alternatives $(1, 1')$ and $(2, 2')$, would add incoherently. However, as we shall show, they give rise to a counter-intuitive interference effect. To demonstrate this result we evaluate the correlation between the photon-number fluctuations $\Delta n(x_C)$ and $\Delta n(x_T)$ measured at equal detection times by the detectors D_C and D_T , respectively, placed at the transverse position x_C and x_T , behind the two-pinhole masks, namely

$$\langle \Delta n(x_C) \Delta n(x_T) \rangle \propto |G^{(1)}(x_C, x_T)|^2. \quad (4)$$

Here,

$$G^{(1)}(x_C, x_T) = Tr[\hat{\rho}_H \hat{E}_C^-(x_C) \hat{E}_T^+(x_T)] \quad (5)$$

is the first-order correlation function calculated at x_C, x_T , where $\hat{E}_d^+(x_d)$ and $\hat{E}_d^-(x_d)$ are, respectively, the positive and negative frequency part of the electric field operator

at the position x_d , namely

$$\hat{E}_d^{(+)}(x_d) = \iota \sqrt{\frac{\hbar\omega}{2\epsilon_0}} \int d\kappa e^{-\omega t} \hat{a}_d(\kappa), \quad (6)$$

where ω is the detected frequency, t is the detection time and $\hat{a}_d(\kappa)$ is the annihilation operator associated with the transverse mode κ , at the detector D_d , with $d = C, T$. By propagating the field from the detector to the source plane, we can write

$$\hat{a}_d(\kappa) = g\{\kappa; S, x_d\} \hat{a}_s(\kappa), \quad (7)$$

where $g\{\kappa; S, x_d\}$ is the Green's function that describes the propagation of the mode κ from the source S to the detector D_d , placed in x_d , and $\hat{a}_s(\kappa)$ is the annihilation operator at the source S associated with the mode κ .

As demonstrated in [Appendix B](#), in the paraxial approximation and by using the conditions given in [Eqs. \(2\) and \(3\)](#), [Eq. \(4\)](#) becomes

$$\langle \Delta n(x_C) \Delta n(x_T) \rangle \propto |G_{1,1'}^{(1)}(x_C, x_T) + G_{2,2'}^{(1)}(x_C, x_T)|^2, \quad (8)$$

where $G_{1,1'}^{(1)}$ and $G_{2,2'}^{(1)}$ indicate the contributions to the correlation measurement coming from the two pairs of paths $(1, 1')$ and $(2, 2')$, respectively; in fact, we have

$$G_{i,j}^{(1)}(x_C, x_T) \propto B_i^*(x_C) B_j(x_T) FT \{|A(x_s)|^2\} [(x_i - x_j)/(2al_{coh})], \quad (9)$$

where $B_i^*(x_C)$ and $B_j(x_T)$ are two phase factors (see [Eq. \(A.8\)](#)), $FT \{|A(x_s)|^2\} [\chi]$ represents the Fourier transform, calculated in χ , of the source intensity profile, which we have assumed to be constant and different from zero only over an extension $2a$ (see [Eq. \(B.7\)](#)) so that $l_{coh} = \lambda z/(2a)$. Hence, on the one hand, due to the conditions in [Eq. \(2\)](#), the contributions $G_{1,2'}^{(1)}$ and $G_{2,1'}^{(1)}$ are null; on the other hand, the conditions in [Eq. \(3\)](#) guarantee that the contribution $G_{i,i'}^{(1)}$ with $i = 1, 2$, are maximum:

$$\begin{aligned} G_{i,i'}^{(1)}(x_C, x_T) &\propto a B_i^*(x_C) B_{i'}(x_T), \\ G_{1,2'}^{(1)}(x_C, x_T) &= G_{2,1'}^{(1)}(x_C, x_T) = 0. \end{aligned} \quad (10)$$

Therefore the correlation between the fluctuations of the number of photons depends on the *interference* between the first-order correlation functions associated with the pairs of paths $(1, 1')$ and $(2, 2')$. In fact, these two pairs of paths are *indistinguishable* even if the corresponding pairs of pinholes are separated much further than the coherence length of the source. Such indistinguishability arises from the fact that each contribution $G_{i,j}^{(1)}$ ([Eq. \(9\)](#)), for each of the four possible pairs of paths $(i,j) = (1,1'), (2,2'), (1,2'), (2,1')$, depends only on the relative distance $x_i - x_j$ between the point-like pinholes i and j as compared to the transverse coherence length, and the paths $(1,1')$ and $(2,2')$ are the only ones corresponding to pinholes having a relative distance smaller than the transverse coherence length (conditions [\(2\)](#) and [\(3\)](#)). Therefore only these two pairs of paths have non-zero contribution ([Eq. \(10\)](#)) and interfere ([Eq. \(8\)](#)).

As shown in [Appendix B](#), [Eq. \(8\)](#) can be written as

$$\langle \Delta n(x_C) \Delta n(x_T) \rangle \propto |1 + e^{i\phi(x_1, x_2, x_{1'}, x_{2'}, x_C, x_T)}|^2, \quad (11)$$

where

$$\phi(x_1, x_2, x_{1'}, x_{2'}, x_C, x_T) = \frac{\omega}{2ch}(x_1^2 + x_2^2 - x_{1'}^2 - x_{2'}^2) + \frac{\omega}{cf}(x_C x_2 - x_T x_{2'} - x_C x_1 + x_T x_{1'}), \quad (12)$$

with $1/h = 1/z + 1/f$. In the condition $x_C = x_T$, Eq. (12) reduces to

$$\begin{aligned} \phi_{x_C=x_T}(x_1, x_2, x_{1'}, x_{2'}, x_C) &= \frac{\omega}{2ch}[(x_1^2 - x_2^2) - (x_{1'}^2 - x_{2'}^2)] \\ &\quad - \frac{x_C \omega}{cf}[(x_1 - x_2) - (x_{1'} - x_{2'})]. \end{aligned}$$

Interestingly, the phase $\phi_{x_C=x_T}(x_1, x_2, x_{1'}, x_{2'}, x_C)$ consists of two terms: each term depends on the difference between the relative positions (the values of the positions are squared in the first term) of the pinholes in each mask; furthermore, the second term depends on the detector position $x_C = x_T$. Therefore, the measured interference provides simultaneous information about the two relative positions of the pinholes in the two masks. For example, this information can be retrieved by varying the positions of both detectors. This would not be possible by measuring the intensity separately at the two interferometer output ports, since no first-order interference can be observed. This effect is of interest for imaging and metrology applications.

3. Quantum gate simulation

In this section we demonstrate that the novel physical effect described by Eq. (8) can be exploited for simulating a controlled- U_ϕ gate, with U_ϕ described by the matrix

$$U_\phi := \begin{pmatrix} 0 & e^{i\phi} \\ e^{i\phi} & 0 \end{pmatrix}. \quad (13)$$

Let us start by describing a *genuine* controlled- U_ϕ gate. Given two-qubit input states $|\phi_C\rangle_C |\phi_T\rangle_T$, where

$$|\phi_C\rangle_C := \cos \phi_C |H\rangle_C + \sin \phi_C |V\rangle_C,$$

and

$$|\phi_T\rangle_T := \cos \phi_T |H\rangle_T + \sin \phi_T |V\rangle_T,$$

the controlled- U_ϕ gate operates on the input states, by giving the following output entangled state [18]

$$|\psi\rangle = \cos \phi_C |H\rangle_C |\phi_T\rangle_T + e^{i\phi} \sin \phi_C |V\rangle_C |\phi_T^{(F)}\rangle_T,$$

where

$$|\phi_T^{(F)}\rangle_T := \sin \phi_T |H\rangle_T + \cos \phi_T |V\rangle_T.$$

The polarization-dependent joint detection probability associated with the state $|\psi\rangle$ is

$$P_{U_\phi} := |\langle \theta_C, \theta_T | \psi \rangle|^2 = \left| \cos \phi_C \cos \theta_C \cos(\phi_T - \theta_T) + e^{i\phi} \sin \phi_C \sin \theta_C \sin(\phi_T + \theta_T) \right|^2. \quad (14)$$

In particular, for $\phi = 0$ the controlled- U_ϕ gate reduces to a CNOT gate [18] and the polarization-dependent joint detection probability in Eq. (14) becomes

$$P_{\text{CNOT}} := |\langle \theta_C, \theta_T | \psi \rangle|^2 = |\cos \phi_C \cos \theta_C \cos (\phi_T - \theta_T) + \sin \phi_C \sin \theta_C \sin (\phi_T + \theta_T)|^2. \quad (15)$$

In order to simulate a controlled- U_ϕ gate we propose the interferometer in Fig. 2 which is identical to the one in Fig. 1, with the only addition of polarization optics. The interferometer consists of three parts: the first one prepares the initial polarization state in the “control” input port \mathcal{C} and in the “target” input port \mathcal{T} ; the second one implements polarization transformations along the control and target output channels; the final part consists of the measurement process.

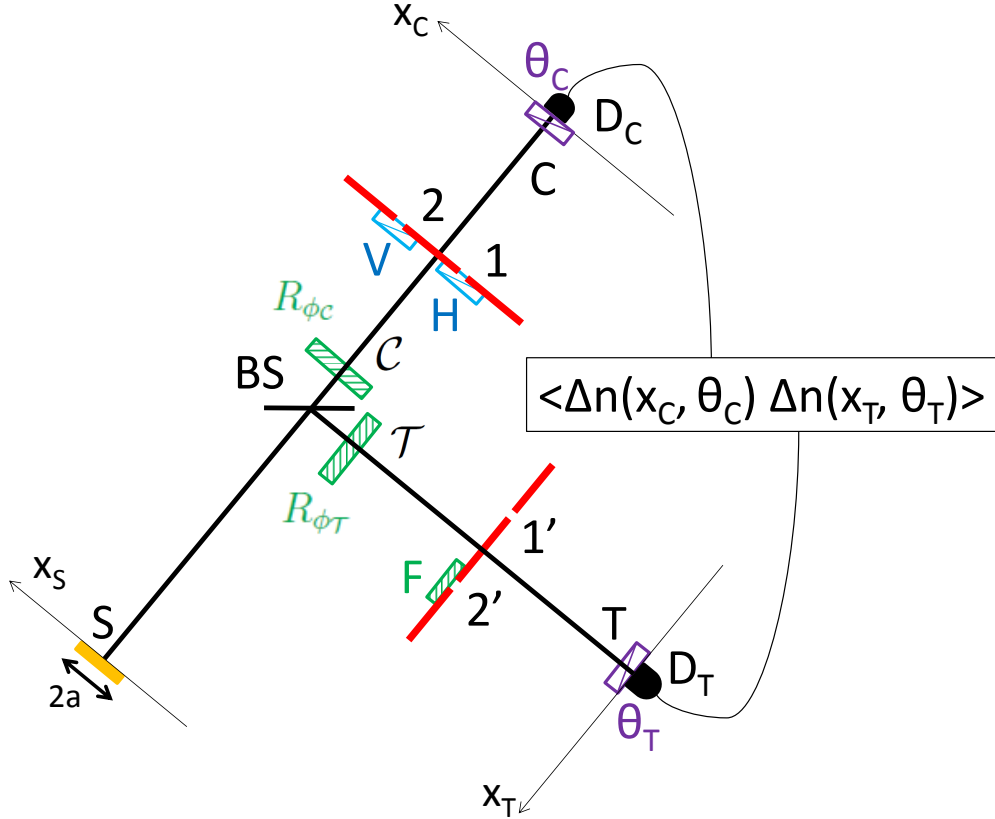


Figure 2. Interferometer for the simulation of controlled- U_ϕ gates. In the first part of the interferometer, the initial polarization state of the light is prepared. The second part, from the ports \mathcal{C} and \mathcal{T} to the ports \mathcal{C} and \mathcal{T} , respectively, performs a polarization-dependent transformation. Correlation measurements in the fluctuations of the number of photons are performed at the interferometer output. R_{ϕ_C} and R_{ϕ_T} are two half-wave plates that rotate the polarization of the angles ϕ_C and ϕ_T , respectively; F is a half-wave plate implementing a flip from the horizontal (H) polarization to the vertical (V) polarization and vice versa; H , V , θ_C and θ_T represent the polarization directions for the corresponding polarizers.

In the first part of the setup the H-polarized chaotic light impinges on a balanced

non-polarizing beam splitter and then propagates through two half-wave plates R_{ϕ_C} and R_{ϕ_T} .

The second part of the setup consists of a “control” path, connecting the ports \mathcal{C} and C , and a “target” path, connecting the ports \mathcal{T} and T . Similar to the setup in Fig. 1, both in the control and in the target paths light goes through identical two-pinhole masks. However, in the control path, two polarizers oriented along the H and V directions are placed just before pinholes 1 and 2, respectively, while in the target path a half-wave plate oriented at $\pi/4$ is placed just before the pinhole $2'$.

Let us now describe the detection process. A polarizer, oriented along the direction $\boldsymbol{\theta}_d := (\cos \theta_d \quad \sin \theta_d)^T$, with $d = C, T$, is placed in front of each detector. A polarization-dependent correlation measurement between the fluctuations of the number of photons $\Delta n(x_C, \theta_C)$ and $\Delta n(x_T, \theta_T)$, detected, respectively, by D_C and D_T , is then performed.

As shown in Appendix C, if the conditions given in Eqs. (2) and (3) are satisfied, in paraxial approximation the correlation between the fluctuations of the number of photons is proportional to the joint detection probability typical of a controlled- U_ϕ gate, namely

$$\langle \Delta n(x_C, \theta_C) \Delta n(x_T, \theta_T) \rangle \propto \left| G_{1,1'}^{(1)}(x_C, \theta_C, x_T, \theta_T) + G_{2,2'}^{(1)}(x_C, \theta_C, x_T, \theta_T) \right|^2 \propto P_{U_\phi}, \quad (16)$$

with $\phi(x_1, x_2, x_{1'}, x_{2'}, x_C, x_T)$ as defined in Eq. (12). Here, we find again two interfering contributions $G_{1,1'}^{(1)}$ and $G_{2,2'}^{(1)}$, associated with the propagation through the two pairs of pinholes (1, 1') and (2, 2'), respectively. However, different from the setup in Fig. 1, these interfering contributions are now polarization dependent. In particular:

- (A) the control path 1, associated with the polarization mode H, is correlated with the target path 1', where the polarization is not modified;
- (B) the control path 2, associated with the polarization mode V, is correlated with the target path 2', where the polarization is flipped from H to V, and vice versa.

Interestingly, the resulting second-order interference pattern is proportional to the probability P_{U_ϕ} associated with a controlled- U_ϕ gate, with ϕ defined in Eq. (12). In particular, when

$$|\phi(x_1, x_2, x_{1'}, x_{2'}, x_C, x_T)| \ll 1, \quad (17)$$

Eq. (16) reduces to

$$\langle \Delta n(x_C, \theta_C) \Delta n(x_T, \theta_T) \rangle \propto P_{CNOT},$$

with P_{CNOT} defined in Eq. (15), leading to the simulation of a CNOT gate operation. The condition reported in Eq. (17) can be experimentally obtained, for example, by performing the detections at equal positions $x_C = x_T$ in the condition

$$|x_{i'}^2 - x_i^2| \ll \frac{2l_{coh}ah}{\pi z},$$

for $i = 1, 2$, with $l_{coh} = \lambda z / (2a)$.

4. Toward higher order correlations

The basic idea described in the previous section can be generalized in order to simulate higher-order entanglement correlations. To this end, we modify the setup of Fig. 2 by replacing the two masks with two Mach-Zehnder-like interferometer, as shown in Fig. 3. It is worth noticing that this modified setup is the spatial equivalent of the setup proposed in [10] in the temporal domain. In fact, by employing the technique proposed in [10], several such interferometers can be combined to simulate higher-order networks. In this perspective, it is worth demonstrating that also the interferometer in Fig. 3 can simulate controlled- U_ϕ gates and, in particular, a CNOT gate.

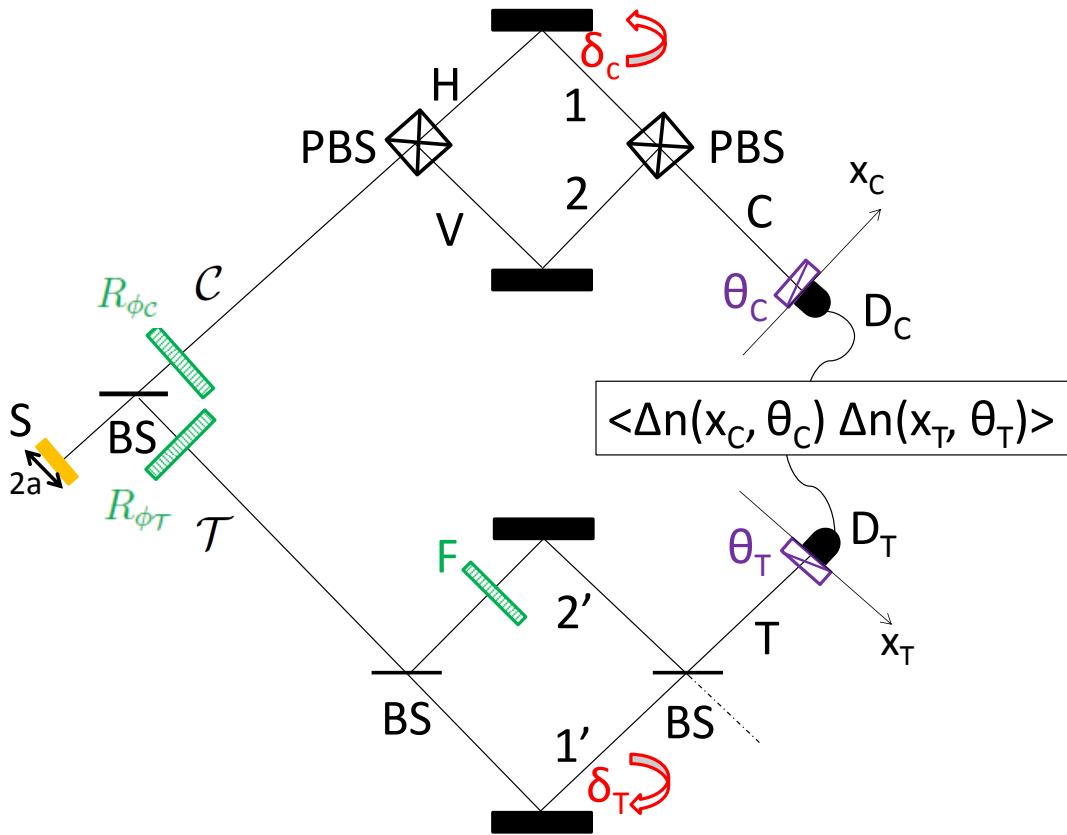


Figure 3. Modified version of the interferometer reported in Fig. 2 for the simulation of controlled- U_ϕ gates. This interferometric configuration can be used as building blocks for the implementation of more general higher-order networks [10].

As mentioned above, the two masks of the scheme in Fig. 2 are substituted by two interferometers: the “control” interferometer, connecting the input port C with the output port C , and the “target” interferometer, connecting the input port T with the output port T . The control interferometer consists of two polarizing beam splitters and two tiltable mirrors. The mirror in one path is tilted by an angle δ_C with respect to the alignment position ($\delta_C = 0$) corresponding to the two interferometric paths 1 and 2 to have equal lengths. Hence the tilting angle δ_C determines the difference between the

optical paths 1 and 2, and the PBS plays the role of the polarizers placed on the mask in arm C of the setup reported in Fig. 2. The target interferometer is a standard Mach-Zehnder interferometer, with a half wave plate F , analogously to the one employed in the setup in Fig. 2 along the path $2'$. Similar to the conditions (Eqs. (2) and (3)) imposed in the setups of Figs. 1 and 2, the tilting angles δ_C and δ_T satisfy, in the small angle approximation, the conditions

$$|\delta_C| \gg \frac{l_{coh}}{2\bar{z}}, \quad |\delta_T| \gg \frac{l_{coh}}{2\bar{z}}, \quad (18)$$

$$|\delta_C - \delta_T| \ll \frac{l_{coh}}{2\bar{z}}, \quad (19)$$

where \bar{z} is the longitudinal distance from the mirrors to the detectors. As in Fig. 1, we shall measure the correlation in the fluctuations of the number of photons detected by D_C and D_T , which are placed at the same longitudinal distance z from the source.

As demonstrated in Appendix E, in the condition

$$|x_C - x_T| \ll l_{coh} \quad (20)$$

and in the paraxial approximation, the correlation between the photon-number fluctuations reads

$$\langle \Delta n(x_C, \theta_C) \Delta n(x_T, \theta_T) \rangle \propto \left| G_{1,1'}^{(1)}(x_C, \theta_C; x_T, \theta_T) + G_{2,2'}^{(1)}(x_C, \theta_C; x_T, \theta_T) \right|^2 \propto P_{U_\phi}, \quad (21)$$

where P_{U_ϕ} is defined in Eq. (14), with ϕ given by the corresponding expression of Eq. (12), namely

$$\phi(x_C, x_T, \delta_C, \delta_T) = \frac{2\omega}{cz} \left[\bar{z}^2 (\delta_C^2 - \delta_T^2) + \bar{z} (x_C \delta_C - x_T \delta_T) \right].$$

Hence, similar to the setup in Fig. 2, the interference between the two pairs of paths $(1, 1')$ and $(2, 2')$ leads to the simulation of a controlled- U_ϕ operation, with U_ϕ defined in Eq. (13). Also in this case the operation of a CNOT gate can be simulated if

$$|\phi(x_C, x_T, \delta_C, \delta_T)| \ll 1,$$

which can be achieved experimentally by choosing

$$|\delta_C^2 - \delta_T^2| \ll \frac{l_{coh} a}{2\bar{z}^2 \pi},$$

and

$$|x_C \delta_C - x_T \delta_T| \ll \frac{l_{coh} a}{2\bar{z} \pi},$$

with $l_{coh} = \lambda z / (2a)$.

5. Discussions

We have theoretically demonstrated a second-order spatial interference effect emerging from correlation measurements in the photon-number fluctuations. We have showed that

interference occurs between two pairs of correlated paths, namely those associated with the pairs of the pinholes (Figs. 1 and 2) or paths $(1, 1')$ and $(2, 2')$. Interestingly, such interference occurs even if the two pairs of pinholes are separated by a distance much larger than the transverse coherence length l_{coh} of the source. Indeed, the interference between the pairs of paths $(1, 1')$ and $(2, 2')$ arises from the fact that the two correlated paths 1 and $1'$ (or 2 and $2'$) in the first (or second) pair correspond to the propagation through two pinholes, 1 and $1'$ (or 2 and $2'$), separated by a distance smaller than the transverse coherence length. This is not the case for the other two possible pairs of paths, which therefore cannot contribute to the interference. Furthermore, we have shown that the resulting interference pattern provides information on the exact position of the four pinholes, despite this information could have not been retrieved by first-order measurements at the two output channels of the interferometer. Therefore, this effect may have applications in high-precision metrology and imaging [12, 37, 38, 39].

In addition, we have demonstrated that this novel spatial interference phenomenon can be used to simulate a particular class of controlled- U_ϕ gates. This includes the simulation of a CNOT gate, which was recently implemented experimentally [40].

Finally, we have introduced a modified setup for controlled- U_ϕ gate simulations which can be used as a building block for more general higher-order interferometric networks. This scheme enables to simulate, on demand, arbitrary-order entanglement correlations, which could be of interest for applications in metrology as well as for the implementation of novel optical algorithms [41, 42, 43, 44].

In conclusion the proposed spatial interference phenomenon provides a deeper understanding of the physics of the spatial coherence and multi-photon interference, while leading to several potential applications in information processing, including high-precision metrology and imaging.

Acknowledgments

M.C. and V.T. would like to thank J. Seiler for useful discussions. This work has been supported by P.O.N. RICERCA E COMPETITIVITA' 2007-2013 - Avviso n. 713/Ric. del 29/10/2010, Titolo II - "Sviluppo/Potenziamento di DAT e di LPP" (project n. PON02-00576-3333585). V.T. acknowledges the support of the German Space Agency DLR with funds provided by the Federal Ministry of Economics and Technology (BMW) under grant no. DLR 50 WM 1556

Appendix A. Green's function for the setup in Fig. 1

Let us calculate explicitly the Green's propagator for the setup shown in Fig. 1. We have [13, 45, 46]

$$g\{\kappa; S, x_d\} = \frac{1}{\sqrt{2}} e^{i\varphi(d)} \int dx_s dx_M A(x_s) M(x_M) \quad (\text{A.1})$$

$$\times e^{i\kappa x_s} \left\{ \frac{-i\omega}{2\pi c} \frac{e^{i\omega z/c}}{z} \mathcal{G}(|x_s - x_M|)_{[\omega/(cz)]} \right\} \left\{ \frac{-i\omega}{2\pi c} \frac{e^{i\omega f/c}}{f} \mathcal{G}(|x_M - x_d|)_{[\omega/(cf)]} \right\},$$

where $A(x_s)$ is the source amplitude profile, $M(x_M)$ is the mask transfer function defined for simplicity by

$$M(x_M) := \sum_j \delta(x_M - x_j), \quad (\text{A.2})$$

with $j = 1, 2$ for the upper mask and $j = 1', 2'$ for the lower mask, $\mathcal{G}(|\alpha|)_{[\beta]}$ is the Fresnel propagator

$$\mathcal{G}(|\alpha|)_{[\beta]} = e^{i\frac{\beta}{2}|\alpha|^2} \quad (\text{A.3})$$

and the factor $\frac{1}{\sqrt{2}} e^{i\varphi(d)}$ takes into account the propagation through the beam splitter, with the assumption that $\varphi(C) = 0$ for the transmitted ray and $\varphi(D) = \pi$ for the reflected ray.

Let us remind the properties of the Fresnel propagator:

$$\begin{aligned} \mathcal{G}^*(|\alpha|)_{[\beta]} &= \mathcal{G}(|\alpha|)_{[-\beta]} \\ \mathcal{G}(|\alpha + \alpha'|)_{[\beta]} &= \mathcal{G}(|\alpha|)_{[\beta]} \mathcal{G}(|\alpha'|)_{[\beta']} e^{i\beta\alpha\alpha'}. \end{aligned} \quad (\text{A.4})$$

By using the second property of Eq. (A.4) in Eq. (A.1), we have

$$g\{\kappa; S, x_d\} = -\frac{1}{\sqrt{2}} e^{i\varphi(d)} \left(\frac{\omega}{2\pi c} \right)^2 \frac{e^{i\omega(z+f)/c}}{zf} \int dx_s dx_M A(x_s) M(x_M) e^{i\kappa x_s} \mathcal{G}(|x_s|)_{[\omega/(cz)]}$$

$$\times \mathcal{G}(|x_M|)_{[\omega/(cz)]} e^{-i\omega x_s x_M / (zc)} \mathcal{G}(|x_M|)_{[\omega/(cf)]} \mathcal{G}(|x_d|)_{[\omega/(cf)]} e^{-i\omega x_d x_M / (fc)}. \quad (\text{A.5})$$

Now using the first property of Eq. (A.4) in Eq. (A.5) and rearranging the result, we obtain

$$g\{\kappa; S, x_d\} = -\frac{1}{\sqrt{2}} \left(\frac{\omega}{2\pi c} \right)^2 \frac{e^{i[\varphi(d) + \omega(z+f)/c]}}{zf} \mathcal{G}(|x_d|)_{[\omega/(cf)]}$$

$$\times \int dx_M M(x_M) \mathcal{G}(|x_M|)_{[\omega/(ch)]} e^{-i\omega x_d x_M / (cf)}$$

$$\times \int dx_s A(x_s) \mathcal{G}(|x_s|)_{[\omega/(cz)]} e^{i[\kappa - \omega x_M / (cz)] x_s}, \quad (\text{A.6})$$

where

$$\frac{1}{h} = \frac{1}{z} + \frac{1}{f}.$$

Considering the mask transfer function (Eq. (A.2)), Eq. (A.6) becomes

$$g\{\kappa; S, x_d\} = \sum_j B_j(x_d) \int dx_s A(x_s) \mathcal{G}(|x_s|)_{[\omega/(cz)]} e^{i[\kappa - \omega x_j/(zc)]x_s}, \quad (\text{A.7})$$

where

$$B_j(x_d) = -\frac{1}{\sqrt{2}} \left(\frac{\omega}{2\pi c} \right)^2 \frac{e^{i[\varphi(d) + \omega(z+f)/c]}}{zf} \mathcal{G}(|x_d|)_{[\omega/(cf)]} \mathcal{G}(|x_j|)_{[\omega/(ch)]} e^{-i\omega x_d x_j/(fc)}. \quad (\text{A.8})$$

Equation(A.7) shows that the Green's function is the summation of two contributions, one from each pinhole in the mask:

$$g\{\kappa; S, x_d\} = \sum_j g_j\{\kappa; S, x_d\}, \quad (\text{A.9})$$

with

$$g_j\{\kappa; S, x_d\} = B_j(x_d) \int dx_s A(x_s) \mathcal{G}(|x_s|)_{[\omega/(cz)]} e^{i[\kappa - \omega x_j/(zc)]x_s},$$

the Green's function from the source S to the detector D_d , through the pinhole located in x_j .

Appendix B. Correlation function for the setup in Fig. 1

In the present appendix we present a detailed calculation to obtain Eqs. (8) and (11).

By substituting in Eq. (5) the result obtained by inserting the Green's function given by Eq. (A.9) and (A.10) into the electric field given by Eq. (6) and Eq. (7), we obtain:

$$G^{(1)}(x_C, x_T) = \sum_{\substack{i=1,2 \\ j=1',2'}} |K|^2 Tr \left[\hat{\rho}_H \int d\kappa d\kappa' g_i^*\{\kappa; S, x_C\} g_j\{\kappa'; S, x_T\} \hat{a}_s^+(\kappa) \hat{a}_s(\kappa') \right], \quad (\text{B.1})$$

where $K = i\sqrt{\frac{\hbar\omega}{2\epsilon_0}}$. We can define the pairs of paths as

$$G_{i,j}^{(1)}(x_C, x_T) = |K|^2 Tr \left[\hat{\rho}_H \int d\kappa d\kappa' g_i^*\{\kappa; S, x_C\} g_j\{\kappa'; S, x_T\} \hat{a}_s^+(\kappa) \hat{a}_s(\kappa') \right], \quad (\text{B.2})$$

in such a way that Eq. (B.1) can be written as:

$$G^{(1)}(x_C, x_T) = \sum_{\substack{i=1,2 \\ j=1',2'}} G_{i,j}^{(1)}(x_C, x_T). \quad (\text{B.3})$$

By using the property of chaotic sources [35]

$$Tr \left[\hat{\rho} a^+(\kappa) a(\kappa') \right] = \langle n_\kappa \rangle \delta(\kappa - \kappa'), \quad (\text{B.4})$$

Eq. (B.2) reduces to

$$G_{i,j}^{(1)}(x_C, x_T) = K' \int d\kappa g_i^*\{\kappa; S, x_C\} g_j\{\kappa; S, x_T\}, \quad (\text{B.5})$$

with $K' = |K|^2 \langle n_\kappa \rangle$, and $\langle n_\kappa \rangle$ the average photon number in the mode κ , assumed to be constant. By substituting in Eq. (B.5) the results of Eqs. (A.7, A.9), we get

$$\begin{aligned}
G_{i,j}^{(1)}(x_C, x_T) &= K' \int d\kappa g_i^* \{ \kappa; S, x_C \} g_j \{ \kappa; S, x_T \} \\
&= K' B_i^*(x_C) \int dx_s A^*(x_s) e^{i\omega x_i x_s / (cz)} \mathcal{G}^*(|x_s|)_{[\omega/(cz)]} \\
&\quad \times B_j(x_T) \int dx'_s A(x'_s) e^{-i\omega x_j x'_s / (cz)} \mathcal{G}(|x'_s|)_{[\omega/(cz)]} \int d\kappa e^{i\kappa(x'_s - x_s)} \\
&= K' B_i^*(x_C) B_j(x_T) \int dx_s |A(x_s)|^2 e^{i\omega(x_i - x_j)x_s / (cz)} \\
&= K' B_i^*(x_C) B_j(x_T) FT \{ |A(x_s)|^2 \} [\omega(x_i - x_j) / (2\pi cz)],
\end{aligned} \tag{B.6}$$

where $FT \{ |A(x_s)|^2 \} [\chi]$ represents the Fourier transform of the source intensity profile, calculated in χ .

Setting for simplicity the source amplitude profile

$$A(x_s) := \begin{cases} 1 & |x_s| \leq a \\ 0 & |x_s| > a \end{cases}, \tag{B.7}$$

we have that

$$FT \{ |A(x_s)|^2 \} [\omega(x_i - x_j) / (2\pi cz)] = 2a \operatorname{sinc} [\pi(x_i - x_j) / l_{coh}], \tag{B.8}$$

where $l_{coh} = \lambda z / (2a)$.

Based on Eq. (B.8), we have that when $|x_i - x_j| > l_{coh}$, the Fourier transform of the source profile is approximately zero, so that no correlation arises between the detected intensities. On the contrary the correlation reaches its maximum value for $|x_i - x_j| \ll l_{coh}$. Based on the conditions reported in Eqs. (2) and (3), we have that the Fourier Transform is approximately zero for the contributions coming from the pinholes (1, 2') and (2, 1'), while it is approximately equal to $FT \{ |A(x_s)|^2 \} (0)$ for the contributions coming from (1, 1') and (2, 2'). Therefore, by inserting the conditions reported in Eqs. (2) and (3) in Eq. (B.6), and substituting the result in Eq. (B.3), we get

$$G^{(1)}(x_C, x_T) = G_{1,1'}^{(1)}(x_C, x_T) + G_{2,2'}^{(1)}(x_C, x_T);$$

by substituting this result in Eq. (4), we get Eq. (8).

Now, based on Eqs. (2) and (3), and (B.6), the explicit expression of $G^{(1)}(x_C, x_T)$ is given by

$$G^{(1)}(x_C, x_T) = K' FT \{ |A(x_s)|^2 \} (0) [B_1^*(x_C) B_{1'}(x_T) + B_2^*(x_C) B_{2'}(x_T)].$$

By inserting the definition given in Eq. (A.8) we have

$$\begin{aligned}
G^{(1)}(x_C, x_T) &= C_b \mathcal{G}^*(|x_C|)_{[\omega/(cz)]} \mathcal{G}(|x_T|)_{[\omega/(cz)]} \\
&\quad \times [\mathcal{G}^*(|x_{1'}|)_{[\omega/(ch)]} \mathcal{G}(|x_{1'}|)_{[\omega/(ch)]} e^{i\omega/(cf)(x_C x_{1'} - x_T x_{1'})} \\
&\quad + \mathcal{G}^*(|x_{2'}|)_{[\omega/(cn)]} \mathcal{G}(|x_{2'}|)_{[\omega/(cn)]} e^{i\omega/(cf)(x_C x_{2'} - x_T x_{2'})}],
\end{aligned}$$

with $C_b = (\iota/2) [1/(zf)]^2 K' [\omega/(2\pi c)]^4 FT \{|A(x_s)|^2\} (0)$. By plugging in the above result in Eq. (4) and using the definition of the Fresnel propagator (Eq. (A.3)) we have

$$\begin{aligned} \langle \Delta n(x_C) \Delta n(x_T) \rangle &= C'_b \left| e^{-\omega/(ch)(x_1^2 - x_{1'}^2)} e^{\omega/(cf)(x_C x_1 - x_T x_{1'})} \right. \\ &\quad \left. + e^{-\omega/(ch)(x_2^2 - x_{2'}^2)} e^{\omega/(cf)(x_C x_2 - x_T x_{2'})} \right|^2, \end{aligned}$$

where $C'_b = |C_b|^2$, which corresponds to Eq. (11).

Appendix C. Correlation function for the setup in Fig. 2

In the present appendix we present the detailed calculation to obtain Eq. (16).

As depicted in Fig. 2, polarizers oriented at θ_C and θ_T are placed in front of detectors D_C and D_T , respectively. The polarization-dependent correlation between the fluctuations of the photon number, for quasi-monochromatic 1-dim chaotic sources (ρ_S), is given by

$$\langle \Delta n(x_C, \theta_C) \Delta n(x_T, \theta_T) \rangle = |G^{(1)}(x_C, \theta_C; x_T, \theta_T)|^2, \quad (\text{C.1})$$

where

$$G^{(1)}(x_C, \theta_C; x_T, \theta_T) := \text{tr} \left[\hat{\rho}_{S,S'} \left(\boldsymbol{\theta}_C \cdot \hat{\mathbf{E}}_C^{(-)}(x_C) \right) \left(\boldsymbol{\theta}_T \cdot \hat{\mathbf{E}}_T^{(+)}(x_T) \right) \right] \quad (\text{C.2})$$

is the polarization-dependent first-order correlation function, with $\hat{\rho}_{S,S'} = \hat{\rho}_S \otimes \hat{\rho}_{S'}$ the input state of the beam splitter (with $\rho_{S'}$ the state of the source in the unused input port of the beam splitter, not shown in Fig. 2, i.e. $\rho_{S'} = |0\rangle\langle 0|$), and

$$\hat{\mathbf{E}}_d^{(+)}(x_d) = \iota \sqrt{\frac{\hbar\omega}{2\epsilon_0}} \int d\kappa e^{-\omega t} \begin{pmatrix} \hat{a}_d^H(\kappa) \\ \hat{a}_d^V(\kappa) \end{pmatrix} \quad (\text{C.3})$$

the positive frequency part of the electric field at the detector D_d , with $d = C, T$. The field in Eq. (C.3) has been written in the near field approximation and in the hypothesis that the detection time t is the same for both detectors; $\hat{a}_d^{(H)}(\kappa)$ and $\hat{a}_d^{(V)}(\kappa)$ represent the annihilation operators at the detector D_d associated with the H and V polarization modes, respectively, and with the component of the transverse wave vector κ . In Eq. (C.2), $\hat{\mathbf{E}}_d^{(-)}(x_d)$ is the Hermitian conjugate of the field in Eq. (C.3). The electric field defined in Eq. (C.3) can also be written as the sum of the contributions coming from the sources S and S' , namely:

$$\hat{\mathbf{E}}_d^{(+)}(x_d) = \sum_{s=S,S'} \hat{\mathbf{E}}_{d,s}^{(+)}(x_d),$$

where

$$\hat{\mathbf{E}}_{d,s}^{(+)}(x_d) = \iota \sqrt{\frac{\hbar\omega}{2\epsilon_0}} \int d\kappa e^{-\omega t} \mathcal{M}_{d,s}(\kappa) \begin{pmatrix} \hat{a}_s^H(\kappa) \\ \hat{a}_s^V(\kappa) \end{pmatrix} \quad (\text{C.4})$$

is the electric field operator at the detector D_d , written in terms of the annihilation operators $\hat{a}_s^{(H)}(\kappa)$ and $\hat{a}_s^{(V)}(\kappa)$ associated with the input port s of the beam splitter; $\mathcal{M}_{d,s}(\kappa)$ is the matrix describing the propagation from the source s , to the detector D_d for the mode κ .

As depicted in Fig. 2, we suppose the chaotic source ρ_S to be H-polarized; we thus indicate it as ρ_H . In this hypothesis, Eq. (C.2) reduces to

$$G^{(1)}(x_C, \theta_C; x_T, \theta_T) := \text{Tr} \left[\hat{\rho}_H \hat{\mathcal{E}}_{C,S}^-(x_C) \hat{\mathcal{E}}_{T,S}^+(x_T) \right], \quad (\text{C.5})$$

with

$$\hat{\mathcal{E}}_{d,S}^+(x_d) := K \boldsymbol{\theta}_d \cdot \left[\int d\kappa e^{-i\omega t} \mathcal{M}_{d,S}(\kappa) \begin{pmatrix} \hat{a}_S^H(\kappa) \\ 0 \end{pmatrix} \right], \quad (\text{C.6})$$

where $K = i\sqrt{\frac{\hbar\omega}{2\epsilon_0}}$. By defining

$$L_d(\kappa) := (\cos \theta_d \quad \sin \theta_d) \mathcal{M}_{d,S}(\kappa) \begin{pmatrix} 1 \\ 0 \end{pmatrix}, \quad (\text{C.7})$$

Eq. (C.6) can be rewritten as:

$$\hat{\mathcal{E}}_{d,S}^+(x_d) = K \int d\kappa e^{-i\omega t} L_d(\kappa) \hat{a}_S^H(\kappa), \quad (\text{C.8})$$

and Eq. (C.5) becomes:

$$\begin{aligned} G^{(1)}(x_C, \theta_C; x_T, \theta_T) &= |K|^2 \text{Tr} \left[\hat{\rho}_H \int d\kappa d\kappa' L_C^*(\kappa) L_T(\kappa') \hat{a}_S^{+H}(\kappa) \hat{a}_S^H(\kappa') \right] \\ &= K' \int d\kappa L_C^*(\kappa) L_T(\kappa), \end{aligned} \quad (\text{C.9})$$

where we have used the property given in Eq. (B.4).

We calculate $L_C(\kappa)$ and $L_T(\kappa)$, by using the propagation matrices $\mathcal{M}_{d,S}(\kappa)$ (with $d = C, T$), obtained in Appendix D (Eq. (D.12)):

$$\begin{aligned} L_C(\kappa) &:= (\cos \theta_C \quad \sin \theta_C) \mathcal{P}_{C,C}(\kappa) R_{\phi_C} g\{\kappa; S, R_{\phi_C}\} \begin{pmatrix} 1 \\ 0 \end{pmatrix}, \\ L_T(\kappa) &:= (\cos \theta_T \quad \sin \theta_T) i\mathcal{P}_{T,T}(\kappa) R_{\phi_T} g\{\kappa; S, R_{\phi_T}\} \begin{pmatrix} 1 \\ 0 \end{pmatrix}. \end{aligned}$$

Now, by employing the results of Eqs. (D.5), (D.7), (D.8), (D.9) and (D.10), and the property given in Eq. (D.11), we get:

$$L_C(\kappa) = \frac{1}{\sqrt{2}} [g_1\{\kappa; S, x_C\} \cos \theta_C \cos \phi_C + g_2\{\kappa; S, x_C\} \sin \theta_C \sin \phi_C] \quad (\text{C.10})$$

and

$$L_T(\kappa) = \frac{i}{\sqrt{2}} [g_1\{\kappa; S, x_T\} \cos(\theta_T - \phi_T) + g_2\{\kappa; S, x_T\} \sin(\theta_T + \phi_T)], \quad (\text{C.11})$$

with

$$\begin{aligned} g_p\{\kappa; S, x_d\} &= - \left(\frac{\omega}{2\pi c} \right)^2 \frac{e^{i[\omega(z+f)/c]}}{zf} \mathcal{G}(|x_d|)_{[\omega/(cf)]} \mathcal{G}(|x_p|)_{[\omega/(ch)]} e^{-i\omega x_d x_p / (fc)} \\ &\quad \times \int dx_s A(x_s) \mathcal{G}(|x_s|)_{[\omega/(cz)]} e^{i[\kappa - \omega x_p / (zc)] x_s}, \end{aligned} \quad (\text{C.12})$$

the Green's function, in paraxial approximation, describing the propagation of the mode κ from the source S to the point x_d in the plane of the detector D_d , going through the pinhole $p = 1, 2, 1', 2'$. Plugging in the results in Eqs. (C.10) and (C.11), the correlation function of Eq. (C.9) becomes

$$\begin{aligned} G^{(1)}(x_C, \theta_C; x_T, \theta_T) &= \frac{i}{2} K' \int d\kappa \left[\cos \theta_C \cos \phi_C \cos(\theta_T - \phi_T) g_1\{\kappa; S, x_C\} g_{1'}^*\{\kappa; S, x_T\} \right. \\ &\quad + \sin \theta_C \sin \phi_C \sin(\theta_T + \phi_T) g_2\{\kappa; S, x_C\} g_{2'}^*\{\kappa; S, x_T\} \\ &\quad - \cos \theta_C \cos \phi_C \sin(\theta_T + \phi_T) g_1\{\kappa; S, x_C\} g_{2'}^*\{\kappa; S, x_T\} \\ &\quad \left. - \sin \theta_C \sin \phi_C \cos(\theta_T - \phi_T) g_2\{\kappa; S, x_C\} g_{1'}^*\{\kappa; S, x_T\} \right], \end{aligned} \quad (\text{C.13})$$

with $K' = |K|^2 \langle n_\kappa \rangle$. To obtain the result shown in Eq. (16), we insert Eq. (C.13) into Eq. (C.1) after:

- a inserting Eq. (C.12) in Eq. (C.13),
- b carrying on a calculation similar to the one in Eq. (B.6),
- c employing the conditions given in Eqs. (2) and (3).

We get:

$$\begin{aligned} \langle \Delta n(x_C, \theta_C) \Delta n(x_T, \theta_T) \rangle &= C'_b \left| e^{-i\omega/(ch)(x_1^2 - x_{1'}^2)} e^{i\omega/(cf)(x_C x_1 - x_T x_{1'})} \cos \theta_C \cos \phi_C \cos(\theta_T - \phi_T) \right. \\ &\quad \left. + e^{-i\omega/(ch)(x_2^2 - x_{2'}^2)} e^{i\omega/(cf)(x_C x_2 - x_T x_{2'})} \sin \phi_C \sin(\theta_T + \phi_T) \right|^2, \end{aligned}$$

where $C'_b = |(i/2) [1/(zf)]^2 K' [\omega/(2\pi c)]^4 FT \{|A(x_s)|^2\} (0) |^2$.

Appendix D. Propagation matrix $\mathcal{M}(\kappa)$

In this appendix we calculate the propagation matrix $\mathcal{M}_{d,S}(\kappa)$ introduced in Eq. (C.4).

In the setup depicted in Fig. 3, we label as S' the source in the unused input port to the beam splitter (not shown in the Figure). Now, the propagation from the sources S and S' to the beam splitter can be written in matrix form as:

$$P_{ini}(\kappa) := \begin{pmatrix} g\{\kappa; S, BS\} \mathbb{1} & 0 \\ 0 & g\{\kappa; S', BS\} \mathbb{1} \end{pmatrix}, \quad (\text{D.1})$$

where $g\{\kappa; s, BS\}$ is the Green's function propagator in the mode κ from the source s to the beam splitter, with $s = S, S'$; the matrix associated with the beam splitter is

$$BS := \frac{1}{\sqrt{2}} \begin{pmatrix} \mathbb{1} & i\mathbb{1} \\ i\mathbb{1} & \mathbb{1} \end{pmatrix}. \quad (\text{D.2})$$

The propagation from the beam splitter to the half-wave plates (R_{ϕ_C}, R_{ϕ_T}) is described by

$$P_1(\kappa) := \begin{pmatrix} g\{\kappa; BS, R_{\phi_C}\} \mathbb{1} & 0 \\ 0 & g\{\kappa; BS, R_{\phi_T}\} \mathbb{1} \end{pmatrix}, \quad (\text{D.3})$$

where $g\{\kappa; BS, R_{\phi_i}\}$ is the Green's function propagating the mode κ from beam splitter to the half-wave plate R_{ϕ_i} with $i = \mathcal{C}, \mathcal{T}$. The matrix describing the propagation through both of the half-wave plates is

$$\mathcal{R} := \text{diag}(R_{\phi_{\mathcal{C}}}, R_{\phi_{\mathcal{T}}}), \quad (\text{D.4})$$

where

$$R_{\phi_i} := \begin{pmatrix} \cos \phi_i & \sin \phi_i \\ \sin \phi_i & -\cos \phi_i \end{pmatrix}, \quad (\text{D.5})$$

with $i = \mathcal{C}, \mathcal{T}$. The propagation from the half-wave plates $R_{\phi_{\mathcal{C}}}$ and $R_{\phi_{\mathcal{T}}}$ to the points $x_{\mathcal{C}}$ and $x_{\mathcal{T}}$ defined, respectively, on the plane of the detectors $D_{\mathcal{C}}$ and $D_{\mathcal{T}}$ is described by

$$P_2(\kappa) := \begin{pmatrix} \mathcal{P}_{\mathcal{C},\mathcal{C}}(\kappa) & 0 \\ 0 & \mathcal{P}_{\mathcal{T},\mathcal{T}}(\kappa) \end{pmatrix}, \quad (\text{D.6})$$

where

$$\begin{aligned} \mathcal{P}_{\mathcal{C},\mathcal{C}}(\kappa) &:= \int dx_M g\{\kappa; R_{\phi_{\mathcal{C}}}, x_M\} \tilde{M}_{\mathcal{C}}(x_M) g\{\kappa; x_M, x_{\mathcal{C}}\}, \\ \mathcal{P}_{\mathcal{T},\mathcal{T}}(\kappa) &:= \int dx_M g\{\kappa; R_{\phi_{\mathcal{T}}}, x_M\} \tilde{M}_{\mathcal{T}}(x_M) g\{\kappa; x_M, x_{\mathcal{T}}\}, \end{aligned} \quad (\text{D.7})$$

with $g\{\kappa; R_{\phi_i}, x_M\}$ the Green's function propagating the mode κ from the half-wave plate R_{ϕ_i} to the point x_M , defined in the plane of the mask, $g\{\kappa; x_M, x_d\}$ the Green's function propagating the mode κ from the point x_M of the mask to the detector D_d , and

$$\begin{aligned} \tilde{M}_{\mathcal{C}}(x_M) &:= \delta(x_M - x_1)P_H + \delta(x_M - x_2)P_V, \\ \tilde{M}_{\mathcal{T}}(x_M) &:= \delta(x_M - x_{1'})\mathbb{1} + \delta(x_M - x_{2'})F, \end{aligned} \quad (\text{D.8})$$

the overall transmission functions of the masks placed, respectively, in the arm \mathcal{C} and \mathcal{T} of the setup, which take into account both the mask transfer functions (Eq. (A.2), the polarizers

$$P_H := \begin{pmatrix} 1 & 0 \\ 0 & 0 \end{pmatrix}, P_V := \begin{pmatrix} 0 & 0 \\ 0 & 1 \end{pmatrix}, \quad (\text{D.9})$$

and the half-wave plate

$$F := \begin{pmatrix} 0 & 1 \\ 1 & 0 \end{pmatrix}, \quad (\text{D.10})$$

placed on the pinhole 2' (see Fig. 2). By using the property of the Green's function:

$$g\{\kappa; a, b\}g\{\kappa; b, x_d\} = g\{\kappa; a, x_d\}, \quad (\text{D.11})$$

and Eqs. (D.1), (D.2), (D.3), (D.4), (D.6), we obtain that the propagation from the sources (S,S') to the detectors is given by

$$\begin{aligned} \mathcal{M}(\kappa) &:= P_2(\kappa)\mathcal{R} P_1(\kappa) BS P_{ini}(\kappa) = \frac{1}{\sqrt{2}} \\ &\times \begin{pmatrix} \mathcal{P}_{C,\mathcal{C}}(\kappa)R_{\phi_C}g\{\kappa; S, R_{\phi_C}\} & i\mathcal{P}_{C,\mathcal{C}}(\kappa)R_{\phi_C}g\{\kappa; S', R_{\phi_C}\} \\ i\mathcal{P}_{T,\mathcal{T}}(\kappa)R_{\phi_T}g\{\kappa; S, R_{\phi_T}\} & \mathcal{P}_{T,\mathcal{T}}(\kappa)R_{\phi_T}g\{\kappa; S', R_{\phi_T}\} \end{pmatrix} \\ &= \begin{pmatrix} \mathcal{M}_{C,S}(\kappa) & \mathcal{M}_{C,S'}(\kappa) \\ \mathcal{M}_{T,S}(\kappa) & \mathcal{M}_{T,S'}(\kappa) \end{pmatrix}, \end{aligned} \quad (\text{D.12})$$

where $g\{\kappa; s, R_{\phi_i}\}$ is the Green's function propagating the mode κ from the source $s = S, S'$ to the half-wave plate R_{ϕ_i} , with $i = \mathcal{C}, \mathcal{T}$.

Appendix E. Correlation function for the setup in Fig. 3

In the present appendix we present the detailed calculation to obtain Eq. (21).

In the setup depicted in Fig. 3, we label as S' the source in the unused input port to the beam splitter (not shown in the Figure), and consider the following conditions:

- (A) $\hat{\rho}_{S'} = |vac\rangle\langle vac|$,
- (B) $\hat{\rho}_S$ is H-polarized,
- (C) the tilting angles δ_d , with $d = C, T$, are defined in the plane of the interferometer.

The first-order correlation function is still given by Eq. (C.9), with $L_d(\kappa)$ replaced by

$$L'_d(\kappa) := (\cos \theta_d \quad \sin \theta_d) \mathcal{M}'_{d,S}(\kappa) \begin{pmatrix} 1 \\ 0 \end{pmatrix}, \quad (\text{E.1})$$

for $d = C, T$, where $\mathcal{M}'_{d,S}(\kappa)$ is the matrix describing the propagation of the transverse mode κ from the source S to the detector D_d , in the setup of Fig. 3.

We calculate $L'_C(\kappa)$ and $L'_T(\kappa)$ by using the propagation matrices $\mathcal{M}'_{d,S}(\kappa)$ (with $d = C, T$), obtained in Appendix F (Eq. (F.5)):

$$\begin{aligned} L'_C(\kappa) &:= (\cos \theta_C \quad \sin \theta_C) \mathcal{P}'_{C,\mathcal{C}}(\kappa)R_{\phi_C}g\{\kappa; S, R_{\phi_C}\} \begin{pmatrix} 1 \\ 0 \end{pmatrix}, \\ L'_T(\kappa) &:= (\cos \theta_T \quad \sin \theta_T) i\mathcal{P}'_{T,\mathcal{T}}(\kappa)R_{\phi_T}g\{\kappa; S, R_{\phi_T}\} \begin{pmatrix} 1 \\ 0 \end{pmatrix}. \end{aligned}$$

Now by employing the results of Eqs. (D.5), (D.10), (F.3) and (F.4), and the property given in Eq. (D.11), we get:

$$L'_C(\kappa) = \frac{i}{\sqrt{2}} [g_1\{\kappa; S, x_C\} \cos \theta_C \cos \phi_C - g_2\{\kappa; S, x_C\} \sin \theta_C \sin \phi_C] \quad (\text{E.2})$$

and

$$L'_T(\kappa) = -\frac{1}{2\sqrt{2}} [g_1\{\kappa; S, x_T\} \cos(\theta_T - \phi_T) - g_2\{\kappa; S, x_T\} \sin(\theta_T + \phi_T)]. \quad (\text{E.3})$$

Plugging in the results in Eqs. (E.2) and (E.3), the correlation function of Eq. (C.9) (with $L_d(\kappa)$ replaced by $L'_d(\kappa)$) becomes

$$\begin{aligned} G^{(1)}(x_C, \theta_C; x_T, \theta_T) &= K' \int d\kappa L_C^*(\kappa) L'_T(\kappa) = \frac{i}{4} K' \int d\kappa \quad (\text{E.4}) \\ &\times [\cos \theta_C \cos \phi_C \cos(\theta_T - \phi_T) g_1\{\kappa; S, x_C\} g_{1'}^*\{\kappa; S, x_T\} \\ &+ \sin \theta_C \sin \phi_C \sin(\theta_T + \phi_T) g_2\{\kappa; S, x_C\} g_{2'}^*\{\kappa; S, x_T\} \\ &- \cos \theta_C \cos \phi_C \sin(\theta_T + \phi_T) g_1\{\kappa; S, x_C\} g_{2'}^*\{\kappa; S, x_T\} \\ &- \sin \theta_C \sin \phi_C \cos(\theta_T - \phi_T) g_2\{\kappa; S, x_C\} g_{1'}^*\{\kappa; S, x_T\}], \end{aligned}$$

with $K' = |K|^2 \langle n_\kappa \rangle$. In the small angle approximation for δ_C, δ_T , and in the paraxial approximation, we have

$$g_p\{\kappa; S, x_d\} = \frac{-i\omega}{2\pi c} \frac{e^{i\omega z/c}}{z} \int dx_S A(x_S) e^{-i\kappa x_S} e^{-i\omega(x_S - x_{d,p})^2/(2zc)},$$

where $x_{d,p}$ is the detector D_d “effective” transverse position determined by the p -path ($p = 1, 2, 1', 2'$); for the four cases, we have: $x_{C,2} = x_C, x_{T,2'} = x_T, x_{C,1} = x_C + 2\bar{z}\delta_C$ and $x_{T,1'} = x_T + 2\bar{z}\delta_T$, with \bar{z} the longitudinal distance from the mirrors to the detectors. Each term in Eq. (E.4) gives

$$\begin{aligned} &\int d\kappa g_i^*\{\kappa; S, x_C\} g_j\{\kappa; S, x_T\} \\ &\propto \int d\kappa dx_S dx'_S A^*(x_S) A(x'_S) \times e^{-i\kappa(x'_S - x_S)} e^{-i\omega/(2zc) [(x'_S - x_{T,j})^2 - (x_S - x_{C,i})^2]} \\ &= e^{i\omega(x_{C,i}^2 - x_{T,j}^2)/(2zc)} FT \{|A(x_S)|^2\} [\omega(x_{T,j} - x_{C,i})/(2\pi zc)], \end{aligned}$$

where $FT \{|A(x_S)|^2\} [\chi]$ represents the Fourier transform of the source intensity profile calculated in χ and $(i, j) = (\{1, 2\}, \{1', 2'\})$.

Based on the conditions given in Eqs. (18), (19), (20), and in the case considered in Eq. (B.7), we have that

- a For the two pairs of paths labeled by $(1, 1')$ and $(2, 2')$ the Fourier transform reaches approximately its maximum value $FT \{|A(x_S)|^2\} (0)$,
- b For the two pairs of paths labeled by $(1, 2')$ and $(2, 1')$ the Fourier transform is approximately zero.

Equation (E.4) can thus be written as

$$\begin{aligned} G^{(1)}(x_C, \theta_C; x_T, \theta_T) &\simeq C_0 FT \{|A(x_S)|^2\} (0) \\ &\times [\cos \theta_C \cos \phi_C \cos(\theta_T - \phi_T) e^{i\omega[x_C^2 - x_T^2]/(2zc)} + \\ &\sin \theta_C \sin \phi_C \sin(\theta_T + \phi_T) e^{i\omega[(x_C + 2\delta_C \bar{z})^2 - (x_T + 2\delta_T \bar{z})^2]/(2zc)}] \\ &= C'_0 [\cos \theta_C \cos \phi_C \cos(\theta_T - \phi_T) \\ &+ \sin \theta_C \sin \phi_C \sin(\theta_T + \phi_T) e^{i\phi(x_C, x_T, \delta_C, \delta_T)}], \end{aligned}$$

where $C_0 = -(\iota K'/4) [\omega/(2\pi cz)]^2$ and $C'_0 = C_0 FT \{|A(x_S)|^2\}(0)$. By plugging this result in Eq. (C.1), we have

$$\begin{aligned} \langle \Delta n(x_C, \theta_C) \Delta n(x_T, \theta_T) \rangle &= |C'_0|^2 [\cos \theta_C \cos \phi_C \cos(\theta_T - \phi_T) \\ &\quad + \sin \theta_C \sin \phi_C \sin(\theta_T + \phi_T) e^{\iota \phi(x_C, x_T, \delta_C, \delta_T)}]^2, \end{aligned}$$

which is the result reported in Eq. (21).

Appendix F. Propagation matrix $\mathcal{M}'(\kappa)$

In this appendix we calculate the propagation matrix $\mathcal{M}_{d,S}(\kappa)$ introduced in Eq. (E.1).

In the setup of Fig. 3 the propagation from the sources S and S' to the half-wave plates R_{ϕ_C} and R_{ϕ_T} is given by the matrix

$$\begin{aligned} \mathcal{U}_{\text{prep}}(\kappa) &:= \mathcal{R} P_1(\kappa) B S_1 P_{\text{ini}}(\kappa) \\ &= \frac{1}{\sqrt{2}} \begin{pmatrix} R_{\phi_C} g\{\kappa; S, R_{\phi_C}\} & \iota R_{\phi_C} g\{\kappa; S', R_{\phi_C}\} \\ \iota R_{\phi_T} g\{\kappa; S, R_{\phi_T}\} & R_{\phi_T} g\{\kappa; S', R_{\phi_T}\} \end{pmatrix}, \end{aligned} \quad (\text{F.1})$$

where we have used Eqs. (D.1), (D.2), (D.3), (D.4), (D.5) and (D.11), and $g\{\kappa; s, R_{\phi_i}\}$ is the Green's function propagating the mode κ from the $s = S, S'$ source, to the half-wave plate R_{ϕ_i} , with $i = C, T$. The propagation from the half-wave plates R_{ϕ_i} to the points x_C and x_T , defined in the plane of the detectors D_C and D_T respectively, is described by the diagonal matrix

$$\mathcal{P}(\kappa) := \text{diag}(\mathcal{P}'_{C,C}(\kappa), \mathcal{P}'_{T,T}(\kappa)), \quad (\text{F.2})$$

with

$$\mathcal{P}'_{C,C}(\kappa) := \iota \text{diag}(g_1\{\kappa; R_{\phi_C}, x_C\}, -g_2\{\kappa; R_{\phi_C}, x_C\}), \quad (\text{F.3})$$

$$\mathcal{P}'_{T,T}(\kappa) := \frac{\iota}{2} (g_{1'}\{\kappa; R_{\phi_T}, x_T\} \mathbb{1} - g_{2'}\{\kappa; R_{\phi_T}, x_T\} F), \quad (\text{F.4})$$

with F defined in Eq. (D.10). By using the results of Eqs. (F.1) and (F.2), we get

$$\begin{aligned} \mathcal{M}'(\kappa) &:= \mathcal{P}(\kappa) \mathcal{U}_{\text{prep}}(\kappa) = \frac{1}{\sqrt{2}} \\ &\times \begin{pmatrix} \mathcal{P}'_{C,C}(\kappa) R_{\phi_C} g\{\kappa; S, R_{\phi_C}\} & \iota \mathcal{P}'_{C,C}(\kappa) R_{\phi_C} g\{\kappa; S', R_{\phi_C}\} \\ \iota \mathcal{P}'_{T,T}(\kappa) R_{\phi_T} g\{\kappa; S, R_{\phi_T}\} & \mathcal{P}'_{T,T}(\kappa) R_{\phi_T} g\{\kappa; S', R_{\phi_T}\} \end{pmatrix} \\ &= \begin{pmatrix} \mathcal{M}'_{C,S}(\kappa) & \mathcal{M}'_{C,S'}(\kappa) \\ \mathcal{M}'_{T,S}(\kappa) & \mathcal{M}'_{T,S'}(\kappa) \end{pmatrix}. \end{aligned} \quad (\text{F.5})$$

- [1] Hanbury Brown R. and Twiss R.Q. 1956 *Nature* **177** 27–29 ISSN 0028-0836 URL <http://dx.doi.org/10.1038/177027a0>
- [2] Hanbury Brown R. and Twiss R.Q. 1956 *Nature* **178** 1046–1048 URL <http://dx.doi.org/10.1038/1781046a0>
- [3] Glauber R.J. 1963 *Phys. Rev. Lett.* **10**(3) 84–86 URL <http://link.aps.org/doi/10.1103/PhysRevLett.10.84>
- [4] Glauber R.J 2005 *Nobel Lecture* **8** URL http://www.nobelprize.org/nobel_prizes/physics/laureates/2005/glauber-lecture.pdf

- [5] Alley C.O. and Shih Y.H. 1986 *Proceedings of the Second International Symposium on Foundations of Quantum Mechanics in the Light of New Technology* ed of Japan P S (Tokyo) pp 47 – 52
Shih Y.H. and Alley C.O. 1988 *Phys. Rev. Lett.* **61**(26) 2921–2924 URL <http://link.aps.org/doi/10.1103/PhysRevLett.61.2921>
- [6] Hong C.K., Ou Z.Y. and Mandel L. 1987 *Phys. Rev. Lett.* **59**(18) 2044–2046 URL <http://link.aps.org/doi/10.1103/PhysRevLett.59.2044>
- [7] Kim H., Kwon O., Kim W., Kim T. 2006 *Phys. Rev. A* **73**, 023820 URL <http://dx.doi.org/10.1103/PhysRevA.73.023820>
- [8] Liu J., Zhou Y., Wang W., Liu R.F., He K., Li F.L., and Xu Z. 2013 *Optics Express* **21**, 16 URL <http://dx.doi.org/10.1364/OE.21.019209>
- [9] Tamma V. and Laibacher S. 2015 *Phys. Rev. Lett.* **114**(24) 243601 URL <http://link.aps.org/doi/10.1103/PhysRevLett.114.243601>
- [10] Tamma V. and Seiler J. 2015, Multipath Correlation Interference with a Thermal Source *arxiv*: 1503.07369 URL <http://arxiv.org/abs/1503.07369>
- [11] Pittman T.B., Shih Y.H., Strekalov D.V. and Sergienko A.V. 1995 *Phys. Rev. A* **52**(5) R3429–R3432 URL <http://link.aps.org/doi/10.1103/PhysRevA.52.R3429>
- [12] Valencia A., Scarcelli G., D’Angelo M. and Shih Y. 2005 *Phys. Rev. Lett.* **94**(6) 063601 URL <http://link.aps.org/doi/10.1103/PhysRevLett.94.063601>
- [13] D’Angelo M., and Shih Y.H. 2005, *Laser Phys. Lett.* **2**, 567 URL <http://dx.doi.org/10.1002/lapl.200510054>
- [14] Scarcelli G., Berardi V. and Shih Y.H. 2006, *Phys. Rev. Lett.* **96**, 063602 URL <http://dx.doi.org/10.1103/PhysRevLett.96.063602>
- [15] A. Gatti, E. Brambilla, M. Bache, and L. A. Lugiato, *Phys. Rev. A* **70**, 013802 (2004).
- [16] F. Ferri, D. Magatti, A. Gatti, M. Bache, E. Brambilla, and L. A. Lugiato, *Phys. Rev. Lett.* **94**, 183602 (2005).
- [17] Chen H., Peng T. and Shih Y.H. 2013 *Phys. Rev. A* **88**(2) 023808 URL <http://link.aps.org/doi/10.1103/PhysRevA.88.023808>
- [18] Nielsen M. and Chuang I. 2000 *Quantum Computation and Quantum Information* Cambridge Series on Information and the Natural Sciences (Cambridge University Press) ISBN 9780521635035 URL <http://books.google.de/books?id=65FqEKQ0fP8C>
- [19] Tamma V. 2014 *International Journal of Quantum Information* **12** 1560017
- [20] Laibacher S. and Tamma V. 2015 *Phys. Rev. Lett.* **115**(24) 243605 URL <http://link.aps.org/doi/10.1103/PhysRevLett.115.243605>
- [21] Tamma V. and Laibacher S. 2015 *Journal of Modern Optics* 1–5 URL <http://dx.doi.org/10.1080/09500340.2015.1088096>
- [22] Tamma V. and Laibacher S. 2015 *Quantum Inf. Process.* 1–22 ISSN 1570-0755, 1573-1332 URL <http://link.springer.com/10.1007/s11128-015-1177-8>
- [23] D’Angelo M., Chekhova M.V. and Shih Y.H. 2001 *Phys. Rev. Lett.* **87**, 013602 URL <http://dx.doi.org/10.1103/PhysRevLett.87.013602>
- [24] Dowling J., 2008 *Contemporary Physics* **49**, 2 URL <http://dx.doi.org/10.1080/00107510802091298>
- [25] D’Angelo M., Garuccio A. and Tamma V. 2008 *Phys. Rev. A* **77**, 063826 URL <http://dx.doi.org/10.1103/PhysRevA.77.063826>
- [26] Cerf N.J., Adami C. and Kwiat P.G. 1998 *Phys. Rev. A* **57**(3) R1477–R1480 URL <http://link.aps.org/doi/10.1103/PhysRevA.57.R1477>
- [27] Spreew R.J.C. 2001 *Phys. Rev. A* **63**(6) 062302 URL <http://link.aps.org/doi/10.1103/PhysRevA.63.062302>
- [28] Lee K.F. and Thomas J.E. 2002 *Physical Review Letters* **88** 097902 URL <http://link.aps.org/doi/10.1103/PhysRevLett.88.097902>
- [29] Kagalwala K.H., di Giuseppe G., Abouraddy A.F. and Saleh B.E.A. 2013 *Nature Photonics* **7** 72–78

- [30] Peng T. and Shih Y.H. 2015 *EPL* **112**(6) 60006 URL <http://dx.doi.org/10.1209/0295-5075/112/60006>
- [31] Pittman T.B., Fitch M.J., Jacobs B.C. and Franson J.D. 2003 *Phys. Rev. A* **68**(3) 032316 URL <http://link.aps.org/doi/10.1103/PhysRevA.68.032316>
- [32] O'Brien J.L., Pryde G.J., White A.G., Ralph T.C. and Branning D. 2003 *Nature* **426** 264–267 ISSN 0028-0836 URL <http://dx.doi.org/10.1038/nature02054>
- [33] Sanaka K., Kawahara K. and Kuga T. 2002 *Phys. Rev. A* **66**(4) 040301 URL <http://link.aps.org/doi/10.1103/PhysRevA.66.040301>
- [34] Glauber R.J. 2007 *Quantum Theory of Optical Coherence: Selected Papers and Lectures* (John Wiley and Sons) ISBN 978-3-527-40687-6
- [35] Mandel L. and Wolf E. 1995 *Optical Coherence and Quantum Optics* (Cambridge University Press) ISBN 9780521417112 URL <http://books.google.de/books?id=FeBix14iM70C>
- [36] Sudarshan E.C.G. 1963 *Phys. Rev. Lett.* **10**(7) 277–279 URL <http://link.aps.org/doi/10.1103/PhysRevLett.10.277>
- [37] Oppel S, Büttner T, Kok P and von Zanthier J 2012 *Physical Review Letters* **109** ISSN 1079-7114 URL <http://dx.doi.org/10.1103/PhysRevLett.109.233603>
- [38] Pearce M E, Mehringer T, von Zanthier J and Kok P 2015 *Phys. Rev. A* **92**(4) 043831 URL <http://link.aps.org/doi/10.1103/PhysRevA.92.043831>
- [39] Crespi A, Lobino M, Matthews J C F, Politi A, Neal C R, Ramponi R, Osellame R and O'Brien J L 2012 *Applied Physics Letters* **100** 233704 URL <http://scitation.aip.org/content/aip/journal/apl/100/23/10.1063/1.4724105>
- [40] Peng T., Cassano M., Tamma V. and Shih Y.H., in preparation.
- [41] Tamma V 2015 *Quantum Inf. Process.* **11128**:1190 URL <http://link.springer.com/article/10.1007%2Fs11128-015-1190-y>
- [42] Tamma V 2015 *Quantum Inf. Process.* **11128**:1189 URL <http://link.springer.com/article/10.1007/s11128-015-1189-4>
- [43] Tamma V, Zhang H, He X, Garuccio A, Schleich W P and Shih Y 2011 *Phys. Rev. A* **83**(2) 020304 URL <http://link.aps.org/doi/10.1103/PhysRevA.83.020304>
- [44] Tamma V, Zhang H, He X, Garuccio A and Shih Y 2009 *Journal of Modern Optics* **56** 2125–2132 URL <http://dx.doi.org/10.1080/09500340903254700>
- [45] Shih Y.H. 2011 *An Introduction to Quantum Optics* (CRC Press Taylor and Francis group)
- [46] Rubin M.H. 1996 *Phys. Rev. A* **54**, 6 URL <http://dx.doi.org/10.1103/PhysRevA.54.5349>